

## Rheology of bidisperse non-Brownian suspensions

Abhinendra Singh <sup>1,2,3,\*</sup> Christopher Ness,<sup>4</sup> Abhishek K. Sharma,<sup>3</sup> Juan J. de Pablo,<sup>3,5</sup> and Heinrich M. Jaeger<sup>2,6</sup>

<sup>1</sup>*Department of Macromolecular Science and Engineering, Case Western Reserve University, Cleveland, Ohio 10040, USA*

<sup>2</sup>*James Franck Institute, University of Chicago, Chicago, Illinois 60637, USA*

<sup>3</sup>*Pritzker School of Molecular Engineering, University of Chicago, Chicago, Illinois 60637, USA*

<sup>4</sup>*School of Engineering, University of Edinburgh, Edinburgh EH9 3FG, United Kingdom*

<sup>5</sup>*Materials Science Division, Argonne National Laboratory, Lemont, Illinois 60439, USA*

<sup>6</sup>*Department of Physics, The University of Chicago, Chicago, Illinois 60637, USA*



(Received 30 October 2023; accepted 22 August 2024; published 20 September 2024)

We study the rheology of bidisperse non-Brownian suspensions using particle-based simulation, mapping the viscosity as a function of the size ratio of the species, their relative abundance, and the overall solid content. The variation of the viscosity with applied stress exhibits shear-thickening phenomenology irrespective of composition, though the stress-dependent limiting solids fraction governing the viscosity and its divergence point are nonmonotonic in the mixing ratio. Contact force data demonstrate an asymmetric exchange in the dominant stress contribution from large-large to small-small particle contacts as the mixing ratio of the species evolves. Combining a prior model for shear thickening with one for composition-dependent jamming, we obtain a full description of the rheology of bidisperse non-Brownian suspensions capable of predicting effects such as the viscosity reduction observed upon adding small particles to a suspension of large particles.

DOI: [10.1103/PhysRevE.110.034901](https://doi.org/10.1103/PhysRevE.110.034901)

### I. INTRODUCTION

Suspensions of small particles, radius  $a \approx 100 \text{ nm} - 10 \text{ }\mu\text{m}$ , form a class of complex fluids abundant in nature and industry [1–3]. Their widespread use calls for detailed constitutive characterization to enable reliable process design [4], especially in the dense regime where particles and fluid are mixed roughly equally [5]. Under external deformation, these systems, which are apparently simple in composition, exhibit complex rheology including yielding, shear thinning, shear thickening, and jamming [5–7]. Recently this phenomenology has been linked to microscopic physics, specifically constraints that control the relative translation and rotation of interacting particle pairs [8–10]. Shear thickening, for example, represents a crossover from unconstrained to constrained tangential motion as the imposed particle stress  $\sigma$  exceeds a threshold set by the repulsive force  $\sigma_0 \sim F_0/a^2$  [11]. A mean-field approach by Wyart and Cates [12] (WC) captures the transition using a stress-dependent jamming volume fraction  $\phi_J(\sigma)$  interpolating between low ( $\phi_0$ ) and high ( $\phi_m$ ) stress limits, reproducing (in some cases quantitatively) the steady-state rheology [8,13].

The above conceptual framework was devised based on nearly monodisperse suspensions, and most numerical and experimental works that seek to test it reflect this [13–17]. As soon as significant deviations from monodispersity are considered, however, complexity emerges that is not captured by WC [12]. In particular, adding a small quantity of small particles to a system of large ones can reduce the viscosity under shear

[4,18,19], yet in the reverse case when larger particles are added to small ones, only an increase in viscosity is reported [20–22]. Extending the understanding of constraint-controlled rheology to suspensions with size-disperse particles is thus a key open problem. Our approach addresses this challenge in a model system of just two species. Even in this minimal system, particle-size disparity can have a profound effect on the rheology, which, with the exception of a few recent works [16,23–25], has remained largely unexplored, particularly in the context of the frictional interactions. Pednekar *et al.* [24] demonstrated a rheological collapse for polydisperse and bidisperse suspensions once the volume fraction  $\phi$  is scaled with  $\phi_J$ , while Malbranche *et al.* [23] found that the relative viscosity  $\eta_r$  for bidisperse suspensions can be well predicted by the usual power law  $\eta_r = (1 - \phi/\phi_J)^{-2}$  extensively used for quasimonodisperse dense suspensions [12–14]. Guy *et al.* [16] showed that a simple model in which the fraction of frictional contacts enters as a scalar quantity providing a linear interpolation between jamming points fails when one considers the differing stress contributions from different pair classes (large-large, large-small, and small-small). Further, Monti and Rosti [25] linked the reduction in shear-thickening behavior of bidisperse suspensions as compared to the monodisperse case to an increase in  $\phi_J$  exhibited in the suspensions with large size ratio, an idea we develop in this article. More recently, Malbranche *et al.* [26] extended the universal crossover scaling function for bidisperse suspensions originally proposed based on an experimental dataset by Ramaswamy *et al.* [27], demonstrating a collapse for both monodisperse and bidisperse suspensions on the universal curve once scaled with distance from the frictionless jamming for the respective cases.

\*Contact author: [abhinendra.singh@case.edu](mailto:abhinendra.singh@case.edu)

A common feature of the above works is that the rheology of size-disperse suspensions is governed by  $\phi_J$ , which is controlled by (in the bidisperse case) the species size ratio  $\Delta = a_L/a_S$ , their volumetric mixing ratio  $\alpha = N_S a_S^3 / (N_S a_S^3 + N_L a_L^3)$ , and the particle friction coefficient  $\mu$  [28]. Here  $N_L$  and  $N_S$  denote the numbers of large and small particles with respective radii being  $a_L$  and  $a_S$ . Farris [29] proposed a model to predict the viscosity of a multimodal suspension based on the idea that the finer particles behave as a liquid with viscosity governed by their volume fraction, which was recently adapted to polydisperse suspensions by Mwasame *et al.* [30]. Shapiro and Probst [31] used bidisperse glass beads in glycerin and demonstrated that increasing size ratio  $\Delta$  leads to higher  $\phi_J$ . Other studies have also shown a similar decrease in viscosity for concentrated bidisperse suspensions as compared to the monodisperse case for a constant  $\phi$  [32–35].

Previous experimental [28,34,36] and numerical [16,23,24,37–39] studies have shown that, for a constant solids fraction  $\phi$ , the relative suspension viscosity  $\eta_r$  decreases with  $\Delta$  at fixed  $\alpha$  while varying nonmonotonically with  $\alpha$  at fixed  $\Delta$ . This was explained on the basis of  $\phi_J$  being nonmonotonic in  $\alpha$ , for which several models have been proposed [40–44] but a complete micromechanical basis is lacking. In dry granular materials it is understood that  $\phi_J$  depends on  $(\Delta, \alpha, \mu)$  [45], and there have been attempts to relate this to the fraction of smaller particles being rattlers [45,46].

In this article, we systematically explore the role of bidispersity on the rheology of dense, non-Brownian suspensions using an established simulation scheme [11,47]. We explore  $\Delta \leq 12$ ,  $0 < \alpha < 1$ , and  $\phi$  close to the jamming point. Using simulation data, we provide a micromechanical basis for the well-known nonmonotonic dependence  $\eta_r(\alpha)$  for a given  $\phi$ . We show that the nonmonotonic  $\eta_r(\alpha)$  coincides with an exchange of stress contribution dominance from large-large (LL) contacts at small  $\alpha$  to small-small (SS) contacts at large  $\alpha$ , while the stress carried by large-small (LS) contacts is nonmonotonic in  $\alpha$  and vanishes at the extremes. Combining an *ad hoc* extension of WC [12] with a geometric model for  $\phi_J(\Delta, \alpha)$ , we obtain qualitative predictions of the rheology for any bidisperse, shear-thickening, non-Brownian suspension. For simplicity we chose a linear-mixture packing model of the kind described by Yu and Standish [40] (YS), which takes as its inputs only the size ratio of the species and the pure species jamming points. Such a model provides the minimal necessary components with which to obtain the nonmonotonicity of  $\phi_J$  in species mixing ratio predicted by our simulation model, but naturally it omits microphysical details such as lubrication, friction and the critical load. This choice is somewhat arbitrary, though, since due to the modular combination of models we propose one could, in principle, introduce here any packing model relevant to a system of interest. Many such models are present in the literature, one recent example being by Anzivino *et al.* [42]. Using the model, we explore practical settings where small additives are incorporated into suspensions of large particles, rationalizing the counterintuitive finding that increasing  $\phi$  can in some circumstances reduce  $\eta_r$ . Meanwhile, adding large particles to a suspension of small ones always enhances  $\eta_r$ , corroborating experimental findings [21,22].

## II. SIMULATION SCHEME

We model  $N = 6000$  inertialess spheres for  $\Delta \leq 6$  ( $N = 12000$  for  $\Delta = 12$ ) dispersed in density-matched Newtonian liquid under imposed shear stress  $\sigma$  in a constant volume Lees-Edwards periodic domain. Particles interact through short-range hydrodynamic lubrication and contact forces and torques. Forces on particles obey overdamped dynamics, governed by a  $6N$ -dimensional force (and torque) balance between lubrication hydrodynamic ( $F_H$ ) and contact ( $F_C$ ) forces as

$$\vec{0} = \mathbf{F}_H(\mathbf{X}, \mathbf{U}) + \mathbf{F}_C(\mathbf{X}), \quad (1)$$

where particle positions and velocities are represented by  $\mathbf{X}$  and  $\mathbf{U}$ , respectively. In the standard Stokesian dynamics method [48], the resistance matrix diverges as  $1/h$ , where  $h$  is the surface separation between particles. In our work, we allow lubrication breakdown [49], permitting direct contact between particles. To model the direct contacts between particles, we follow Cundall and Strack [50] and the algorithm by Luding [51]. We make use of the lubrication resistance [47] and hence do not use a dashpot explicitly. The tangential  $\mathbf{F}_C^t$  and normal contact  $\mathbf{F}_C^n$  forces between particles satisfy the Coulomb criterion,  $|\mathbf{F}_C^t| \leq \mu |\mathbf{F}_C^n|$ , for compressive normal forces. Here, we use  $\mu = 1$ , which has been shown to yield quantitative comparison with experimentally observed rheology [9,10,47]. Rate dependence is introduced using the so-called critical load model (CLM) [11,52], where frictional force is activated above a threshold normal force  $F_0$  giving a characteristic stress scale of  $\sigma_0 = F_0/a^2$  (here  $a$  is the particle size in the monodisperse limit, and we follow Guy *et al.* [14,16] and assume  $F_0$  to be independent of particle size so that  $\sigma_0 = F_0/a_s^2$  throughout). Such a stress scale originates from an electrostatic double-layer interaction between particles from the polymer coating, as an example. The CLM model can be considered a special case of Debye length  $\lambda$  approaching zero.

Under imposed constant shear stress  $\sigma$ , the suspension flows with the time-dependent shear rate  $\dot{\gamma}(t)$ , and we compute the relative viscosity as  $\eta_r(t) = \sigma/\eta_0\dot{\gamma}(t)$ , with  $\eta_0$  being the liquid viscosity. For high and low values of  $\alpha$  (close to their monodisperse counterparts) and high  $\phi$ , the system is close to jamming; a total of ten simulations were performed for improved statistics. On the other hand, far away from jamming conditions, five realizations were performed. Different initial conditions were generated by placing the nonoverlapping particles with different size ratios  $\Delta$  and volumetric mixing ratios  $\alpha$ . We observe that the steady-state behavior, within fluctuations, is insensitive to different realizations. Finally, rheology data shown in the following are averages of  $\eta_r$  over 5 strain units at steady state after omitting the transient start-up flow, which lasts less than  $O(1)$  strain units. We perform simulations for  $\Delta = 2, 3, 4, 6$ , and  $12$  and  $\alpha = [0.05, 0.9]$ . For small values of  $\Delta$ , we do not find a significant system-size dependence  $N$  on our statistics; the average  $\eta_r$  roughly stays the same by reducing the system size by half (or doubling) the system size, whereas the standard deviation reduces with increasing  $N$ . Further details about the number of large and small particles present in our simulations are given in Table I in the Appendix.

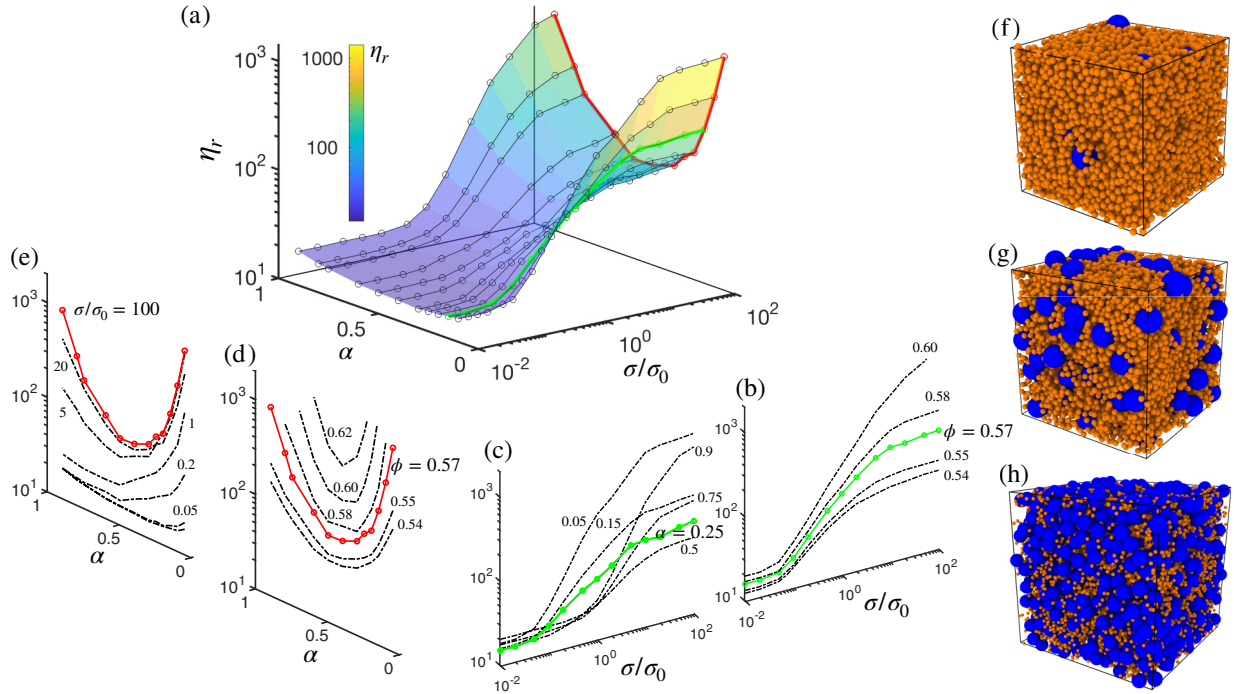


FIG. 1. Effect of mixing small and large particles on the rheology of a model suspension with size ratio  $\Delta = 4$ . Shown are (a) the relative viscosity  $\eta_r$  as a function of the volume ratio of small particles  $\alpha$  and the applied stress  $\sigma/\sigma_0$ , at  $\phi = 0.57$ . Red and green lines represent common data sets across each panel, showing, respectively,  $\eta_r(\alpha)$  for  $\sigma/\sigma_0 = 100$ , and  $\eta_r(\sigma)$  for  $\alpha = 0.25$ . (b)  $\eta_r$  as a function of  $\sigma/\sigma_0$  at fixed  $\alpha = 0.25$  for various  $\phi$ . (c)  $\eta_r$  as a function of  $\sigma/\sigma_0$  at fixed  $\phi = 0.57$  for various  $\alpha$ . (d)  $\eta_r$  as a function of  $\alpha$  for various  $\phi$  at fixed  $\sigma/\sigma_0 = 100$ . (e)  $\eta_r$  as a function of  $\alpha$  for  $\phi = 0.57$  for various  $\sigma/\sigma_0$ . (f)–(h) Snapshots of the simulation at  $\phi = 0.57$ ,  $\sigma/\sigma_0 = 100$ ,  $\Delta = 4$ , and (top-to-bottom)  $\alpha = 0.9, 0.5$ , and  $0.1$ .

### III. RESULTS

**Bidisperse suspension rheology.** Figure 1 shows the effect of  $\alpha$  on the rheology for exemplar data with  $\Delta = 4$ . We present a map of  $(\eta_r, \alpha, \sigma)$  at  $\phi = 0.57$  in Fig. 1(a) showing an overview of the behavior, with planar slices showing (b)  $\eta_r(\sigma/\sigma_0, \phi)$  at  $\alpha = 0.25$ ; (c)  $\eta_r(\sigma/\sigma_0, \alpha)$  at  $\phi = 0.57$ ; (d)  $\eta_r(\alpha, \phi)$  at  $\sigma/\sigma_0 = 100$ ; and (e)  $\eta_r(\alpha, \sigma/\sigma_0)$  at  $\phi = 0.57$ . In Figs. 1(f)–1(h) are snapshots of the simulation at  $\alpha = 0.9, 0.5$ , and  $0.1$ . In Fig 1(b), one observes canonical thickening behavior, qualitatively similar to quasimonodisperse systems showing a stress-mediated transition between two Newtonian plateaus driven by activation of frictional contacts [14, 15, 52]. The viscosities of the plateaus increase with  $\phi$  towards their respective jamming points, i.e., frictionless  $\phi_J^0 \equiv \phi_J(\sigma/\sigma_0 \rightarrow 0) \approx 0.75$  and frictional  $\phi_J^\mu \equiv \phi_J(\sigma/\sigma_0 \rightarrow \infty) \approx 0.65$  limits (these numbers being sensitive to  $\alpha$ ,  $\Delta$ , and  $\mu$ ). In Fig. 1(c) we find that  $\sigma_0$  increases monotonically with  $\alpha$  (since the former is related to the particle size through  $\sigma_0 \sim F_0/a^2$ ), while the frictionless and frictional viscosities measured at  $\sigma/\sigma_0 = 0.01$  and  $\sigma/\sigma_0 = 100$ , respectively, show nonmonotonic dependence on  $\alpha$ . The crossover of these flow curves is a result of the combined effect of bidispersity on  $\sigma_0$  and  $\phi_J$  and is not predicted by models that assume monodispersity. Next, we present data in the  $\eta_r(\alpha)$  plane. Figure 1(d) shows  $\eta_r$  for  $\sigma/\sigma_0 = 100$  as a function of  $\alpha$  for various  $\phi$ . At fixed  $\phi$ ,  $\eta_r$  first decreases with increasing  $\alpha$ , reaching a minimum before increasing again so that  $\eta_r(\alpha = 0) = \eta_r(\alpha = 1)$ . In the limits  $\alpha = 0$  and  $\alpha = 1$ , the suspension is monodisperse

and exhibits identical rheology due to the size invariance of non-Brownian suspensions (when  $\sigma/\sigma_0$  is 0 or  $\infty$ ). The value of  $\alpha$  that minimizes  $\eta_r$  is insensitive to  $\phi$ . The mentioned behavior is consistent with the literature on flowing suspensions [16, 23, 24, 28, 34, 36–39]. However, none of the studies explored jammed states. For  $\phi \geq 0.58$ , the suspension near the extrema  $\alpha = 0$  and  $\alpha = 1$  is jammed, and the window of  $\alpha$  for which  $\eta_r$  is finite decreases with increasing  $\phi$  so that no flow occurs at any  $\alpha$  for  $\phi \geq 0.65$ . Figure 1(e) shows  $\eta_r(\alpha)$  for various  $\sigma/\sigma_0$  at fixed  $\phi = 0.57$ . For  $\sigma/\sigma_0 = 100$ ,  $\eta_r$  at the large and small limits of  $\alpha$  are equal, while for  $\sigma/\sigma_0 \leq 5$ ,  $\eta_r$  is higher for small  $\alpha$  ( $\alpha \rightarrow 0$ ) as compared to larger values ( $\alpha \rightarrow 1$ ). This can be explained based on the relation between  $\sigma_0$  and particle size  $a$ . Since  $\sigma_0 \sim 1/a^2$ ,  $\sigma_0$  increases with  $\alpha$  [Fig. 1(c)] so that the jamming point is governed by friction at lower stress when particles are large.

Figure 2 shows the effect of  $\Delta$  on the jamming points  $\phi_J^0$  and  $\phi_J^\mu$ . In Figs. 2(a) and 2(b) are the variations of  $\phi_J^0$  and  $\phi_J^\mu$  with  $\alpha$ , for  $\Delta = 2, 3, 4, 6$ , and  $12$ , obtained by simulating the limits  $\sigma/\sigma_0 \rightarrow 0$  (lubricated, frictionless state) and  $\sigma/\sigma_0 \rightarrow \infty$  (frictional state) for a range of  $\phi$  and then fitting the viscosity as  $\eta_r = (1 - \phi/\phi_J^{(0,\mu)})^{-2}$  [53]. Both  $\phi_J^0$  and  $\phi_J^\mu$  vary nonmonotonically with  $\alpha$ , with the dependence being more pronounced for increasing  $\Delta$ , which is consistent with previous experimental and numerical findings. Also plotted are  $\phi_J^{(0,\mu)}$  predictions as functions of  $\alpha$  at various  $\Delta$  following the model of Yu and Standish [40], which produces jamming point predictions based on geometry only. Interestingly the

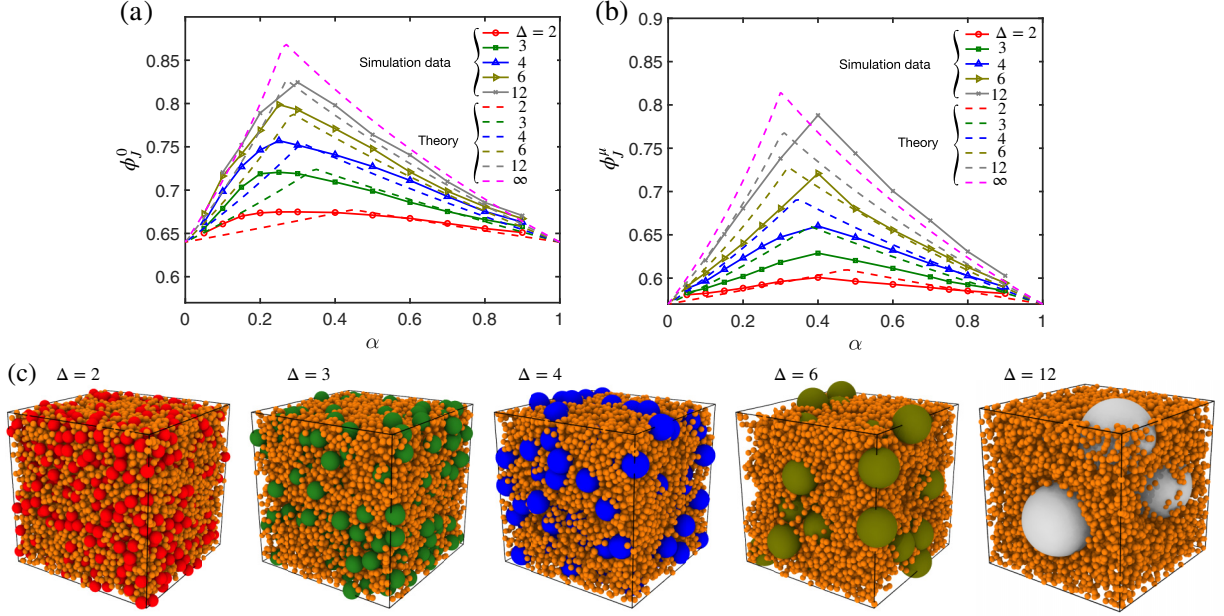


FIG. 2. Role of the particle-size ratio  $\Delta$ . (a) Variation with  $\alpha$  of  $\phi_J^0$ , the jamming point at  $\sigma/\sigma_0 = 0$ , for a range of  $\Delta$ . Solid lines with points represent simulation data; dashed lines show model predictions [40]. (b) Variation with  $\alpha$  of  $\phi_J^\infty$ , the jamming point at  $\sigma/\sigma_0 = \infty$ , for a range of  $\Delta$ . (c) Snapshots of simulations with  $\phi = 0.5, \mu = 1, \alpha = 0.5$ , and (left to right)  $\Delta = 2, 3, 4, 6$ , and  $12$ .

model works better for the frictionless limit ( $\phi_J^0, \sigma/\sigma_0 = 0$ ) as compared to the frictional one ( $\phi_J^\infty, \sigma/\sigma_0 = \infty$ ), likely due to the absence of friction and shear-induced structure in the theory. (Indeed, understanding the disparity in the nature of jamming between frictionless and frictional systems remains an open challenge [54].) In the frictionless case, the simulation data appear to be converging toward the theory for larger values of  $\alpha > 0.4$ . Though for smaller values of  $\alpha$ , discrepancies can be observed. It is also important to mention that testing this for larger  $\Delta$  rapidly becomes computationally intractable. Plotting  $\eta_r$  as a function of  $\sigma/\sigma_0$  for different  $\Delta$  at fixed  $\alpha = 0.5$  and  $\phi = 0.57$  [Fig. 2(c)], one finds the viscosity of both limiting states decreases with increasing  $\Delta$ , as the proximity to jamming is decreased.

**Contribution of different contact types.** We next address the microscopic underpinning of the nonmonotonic  $\eta_r(\alpha)$  reported in Fig. 1 (see also Refs. [16,23,24,28,34,36–39]). In the literature, this behavior has been explained based on the nonmonotonic behavior of  $\phi_J(\alpha)$ , making the distance to jamming ( $\phi_J - \phi$ ) and thus  $\eta_r$  to be nonmonotonic at a given constant  $\phi$ . We use simulation data to separate the stress contributions of different types of contacts LL (large-large), LS (large-small), and SS (small-small). Figure 3(a) shows the viscosity contribution of each contact type scaled with  $\eta_r$  for  $\phi = 0.57$  at  $\sigma/\sigma_0 = 100$  as a function of  $\alpha$  for  $\Delta = 4$ . In the limits  $\alpha = \{0, 1\}$ ,  $\eta_r$  would be purely dominated by LL and SS contacts with the LS contribution being zero in the two limits. At small  $\alpha$ , LL contacts provide the dominant contribution to  $\eta_r$ , while SS contacts take over at large  $\alpha$  as expected. LL decay from 1 at  $\alpha = 0$  (by definition) to  $\approx 0$  for  $\alpha \geq 0.6$ . SS contributions are minimal for  $\alpha \leq 0.2$  and increase to 1 at  $\alpha = 1$ . Notably, the value of  $\alpha$  at which SS contributions begin to increase and LL contributions vanishes

is not symmetric with respect to 0 and 1. The contribution of LS is nonmonotonic and vanishes for  $\alpha = 0$  and 1 and is maximal around  $\alpha = 0.4$  where it contributes  $\approx 75\%$  of the overall viscosity. The LS contribution is the dominant viscosity component for  $\alpha \in \{0.2, 0.75\}$ . Generalizing these findings for different values of  $\phi$ , Figs. 3(b)–3(d) present  $\eta_r$  as a function of  $\phi$  for  $\alpha = 0.15, 0.5$ , and  $0.8$  respectively. We observe that, for small  $\alpha = 0.15$ , the dominant contribution to viscosity originates from LL contacts. The viscosity of large-large particle contacts  $\eta_r^{\text{LL}}$  is nearly 2–3 orders of magnitude larger compared to  $\eta_r^{\text{SS}}$ , while being only 2–3 times larger than  $\eta_r^{\text{LS}}$ . On the other hand, for  $\alpha = 0.8$ ,  $\eta_r^{\text{SS}}$  is 2–3 orders of

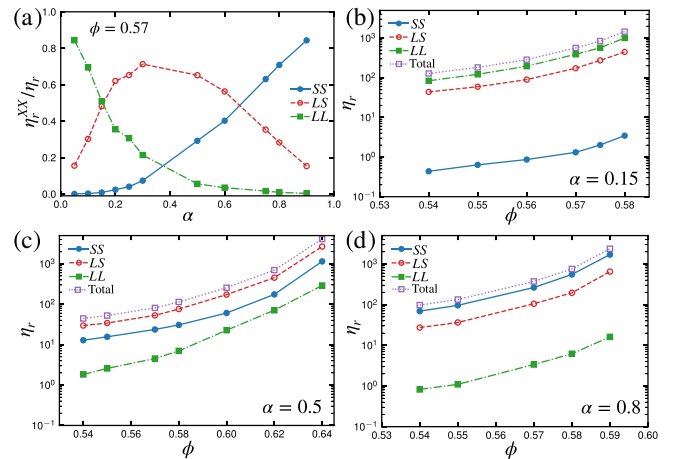


FIG. 3. Viscosity contributions from each contact type. (a) Relative contribution  $\eta_r^{XX}$  to the total viscosity  $\eta_r$  of each contact type (where SS, LS, and LL replace XX) as a function of  $\alpha$ , for  $\phi = 0.57$  and  $\sigma/\sigma_0 = 100$ . (b)–(d) Total viscosity and its contact contributions as a function of  $\phi$  at  $\sigma/\sigma_0 = 100$  for  $\alpha =$  (b) 0.15, (c) 0.5, and (d) 0.8.

magnitude larger than  $\eta_r^{LL}$ . Hence, in the two extreme limits of  $\alpha$ , jamming originates from the dominant contributions from LL and SS components, with LS contributions being the second dominant one. LS components provide the major contribution to viscosity for the intermediate case ( $\alpha = 0.5$ ), followed by SS and LL components being the least significant contributors to viscosity.

*Constitutive model.* Guy *et al.* [16] demonstrated that the WC model and its variants [12,13] as postulated fail to reproduce the bidisperse rheology. Given the qualitative agreement of the dependence of  $\phi_J^0$  and  $\phi_J^\mu$  on  $\alpha$  and  $\Delta$  with the YS model (Fig. 2) and of  $\eta_r(\sigma/\sigma_0)$  with the WC model in our previous nearly monodisperse cases [9,13], we are motivated to construct a combined model to capture the full behavior.

The conventional WC model assumes that the suspension viscosity diverges at the stress-dependent jamming volume fraction as

$$\eta_r(\phi, \sigma/\sigma_0) = [1 - \phi/\phi_m(\sigma/\sigma_0)]^{-2}, \quad (2)$$

where  $\phi_J^0$  and  $\phi_J^\mu$  denote the frictionless and frictional jamming volume fractions. The stress-dependent jamming volume fraction  $\phi_m(\sigma/\sigma_0)$  is postulated as

$$\phi_m(\sigma/\sigma_0) = f(\sigma/\sigma_0)\phi_J^\mu + [1 - f(\sigma/\sigma_0)]\phi_J^0, \quad (3)$$

with the fraction of frictional contacts being expressed as  $f(\sigma/\sigma_0) = \exp(-\sigma_0/\sigma)$ . Here  $\sigma_0$  is the onset stress for thickening.

To extend the WC model to bidisperse systems, we let  $\phi_J^0$  and  $\phi_J^\mu$  be functions of  $\alpha$  and  $\Delta$  as plotted in Figs. 2(a) and 2(b). To incorporate particle-size dependence,  $\sigma_0$  is interpolated in an *ad hoc* way between small- and large-particle limits as  $\sigma_0(\alpha) = F_0/[\alpha a_S + (1 - \alpha)a_L]^2$ . Substituting  $\sigma_0(\alpha)$ ,  $\phi_J^0(\Delta, \alpha)$ , and  $\phi_J^\mu(\Delta, \alpha)$  into Eq. (2), we propose

$$\eta_r(\phi, \sigma/\sigma_0, \Delta, \alpha) = [1 - \phi/\phi_m(\sigma/\sigma_0, \Delta, \alpha)]^{-2}. \quad (4)$$

We note that plotting three-dimensional data together with the model becomes difficult to interpret, and hence only the constitutive model is presented. Using this model we can predict the effect on the rheology of compositional changes. As small (or large) particles are added to an initial suspension of large (or small) particles,  $\alpha$  increases (or decreases) accompanied by an increase in  $\phi$ . First, we consider in Figs. 4(b)–4(d) the effect of adding small particles to a suspension of monodisperse large ones, for  $\Delta = 4$  in the frictional limit ( $\sigma/\sigma_0 = \infty$ ). Here, colors indicate increasing initial volume fraction  $\phi$  from blue to black. Both  $\alpha$  and  $\phi$  increase with the number of small particles. In the case of dense suspensions,  $\eta_r$  ideally increases with  $\phi$ , eventually diverging at the jamming volume fraction [2]. Counterintuitively, for sufficiently large initial  $\phi$  (of large particles), the addition of small particles leads to a decrease in  $\eta_r$ . Even though both  $\phi$  and  $\alpha$  increase as small particles are added, the model predicts that the increase in  $\phi$  is slower than that of  $\phi_m$ , and hence  $(1 - \phi/\phi_m)^{-2}$  decreases. Conversely, the asymmetry in  $\phi_m(\alpha)$  means adding large particles to a packing of small ones leads, more intuitively, to an increase in both  $\phi$  and  $\eta_r$  [Figs. 4(e)–4(g)]. At intermediate  $\sigma/\sigma_0$ ,  $\phi_J$  interpolates between frictionless and frictional values [Fig. 4(h)], and the range of  $\alpha$  for which viscosity reduction appears is broadened [Figs. 4(i) and 4(j)]. Recent experiments have shown that adding large non-Brownian

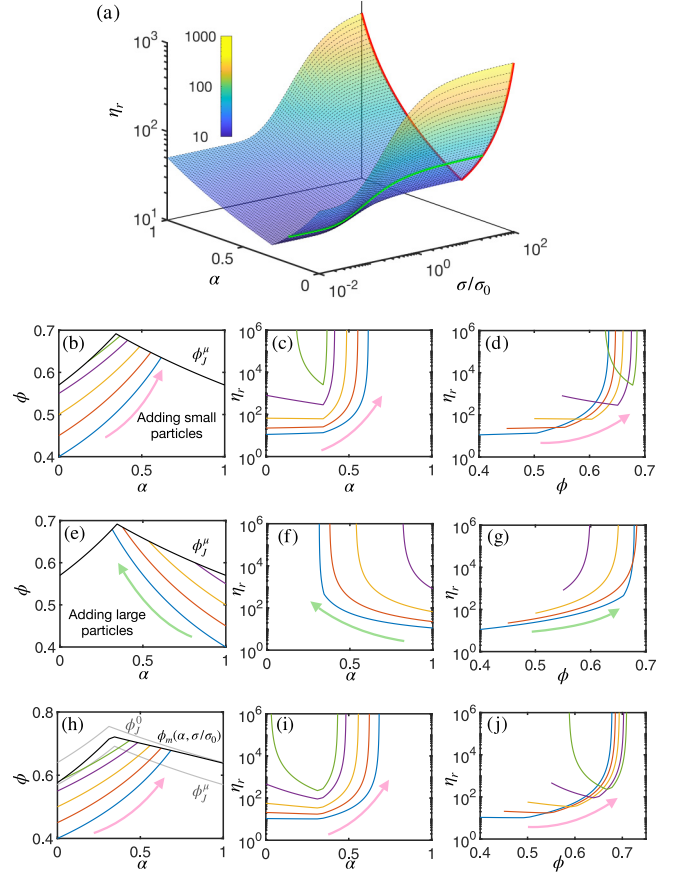


FIG. 4. Constitutive model predictions. (a) Combining the WC model for  $\eta_r(\sigma/\sigma_0)$  with the YS model for  $\phi_J(\alpha, \Delta)$ , one obtains the rheology of bidisperse frictional suspensions. (b)–(j) Colors represent different initial volume fractions  $\phi$  with blue lines representing the lowest initial  $\phi$  and black lines representing jamming volume fractions  $\phi_J^\mu(\alpha)$  and  $\phi_m(\alpha, \sigma/\sigma_0)$ . Colored arrows indicate adding small (pink) and large (green) particles. (b)–(d) Adding small particles to a monodisperse large-particle packing at  $\sigma/\sigma_0 = \infty$ . (b) Variation of  $\phi$  and  $\phi_m$  with  $\alpha$ , and  $\eta_r$  plotted as a function of (c)  $\alpha$  and (d)  $\phi$ . (e)–(g) Adding large particles to a monodisperse small-particle packing at  $\sigma/\sigma_0 = \infty$ . (e) Variation of  $\phi$  and  $\phi_m$  with  $\alpha$ , and  $\eta_r$  plotted as a function of (f)  $\alpha$  and (g)  $\phi$ . (h) and (i) Adding small particles to a monodisperse large-particle packing at intermediate  $\sigma/\sigma_0$ , so that large particles are frictional and small ones are frictionless. (h) Variation of  $\phi$  and  $\phi_J$  with  $\alpha$ , and  $\eta_r$  plotted as a function of (i)  $\alpha$  and (j)  $\phi$ . Also shown in panel (h) in gray are  $\phi_m$  and  $\phi_0$ .

particles to a suspension of small ones leads to enhanced thickening behavior [21,22], consistent with our prediction [Fig. 4(e)] that doing so will always move the system closer to its respective  $\phi_m$ .

#### IV. CONCLUDING REMARKS

In this work, we have studied the rheology of dense bidisperse suspensions by extensive numerical simulations. The simulations presented here consider lubrication hydrodynamics interactions and repulsive normal contact forces, where static frictional force is activated beyond a critical thresh-

old. The rheological flow curves display rate-independent rheology at small stresses ( $\sigma \ll \sigma_0$ ) followed by thickening behavior. The shear-thickening behavior presented depends on the overall volume fraction  $\phi$  as well as packing properties ( $\Delta, \alpha$ ).

For a given large enough  $\phi$  and  $\Delta$ , discontinuous shear thickening is observed around the extreme values of  $\alpha$ , while continuous shear thickening is observed for intermediate  $\alpha$ . Viscosity  $\eta_r$  shows a nonmonotonic dependence as a function of  $\alpha$  for a constant ( $\phi, \sigma/\sigma_0$ ). We address this behavior by separating the stress contributions from different types of contacts, viz., large-large (LL), large-small (LS), and small-small (SS) contacts. We find that at the extreme values of  $\alpha$ , viscosity is dominated by LL and SS contributions with the LS contribution going to zero (by definition). The SS contribution goes much more rapidly as compared to the decrease in SS contribution. The LS contribution is nonmonotonic and carries the majority of stress for intermediate  $\alpha \in \{0.2, 0.7\}$  values.

We have shown that an existing constitutive relation for rate-dependent rheology (WC [12]) can be combined in an *ad hoc* way with a geometric model by Yu and Standish [40] to obtain a qualitative picture of the rheology of bidisperse suspensions, and further work is needed in this direction for a quantitative comparison. We emphasize that using the geometric model by Yu and Standish [40] is purely a choice; many other models [41,42] should yield similar results, perhaps yielding better qualitative predictions for specific systems. Our ansatz for  $\sigma_0(\alpha)$  is not strictly in accordance with WC [12], in the sense that the order parameter  $f$  can no longer represent the fraction of contacts that are frictional (see Ref. [16] for more details), in the sense that we did not explicitly explore different types of frictional contacts (LL, LS, and SS types). Nonetheless, our model predicts novelty in the rheology that is present in reality but unaddressed by WC [12], specifically that adding small particles to a system of large ones can counterintuitively decrease the viscosity, whereas in the opposite case adding large particles to small particles always leads to an increase in  $\eta_r$ .

We show additionally that the nonmonotonic dependence of relative viscosity  $\eta_r$  on  $\alpha$  for constant  $\phi$  (as reported by Refs. [23,24,28,36]) can be understood by delineating the stress contributions of each type of contact, and our results suggest that the rheology at  $\Delta = 12$  is already close to the  $\Delta \rightarrow \infty$  limit, so the predictions made here will be useful across bidisperse systems of arbitrary size ratio. The consequences of these results for more complex systems, especially polydisperse samples [30] in which colloidal forces may become relevant [55], are broad. In particular, our results provide a direction towards the limiting case of predicting the rheology of mixtures where larger additives are included in a continuous background phase of much smaller particles [20]. Recent work by Pednekar *et al.* [24] demonstrated that the rheology of a polydisperse suspension (viscosity, normal stresses, and particle pressure) can be represented by an equivalent bidisperse suspension. This work was in parts inspired by previous works by Desmond and Weeks [56] and Ogarko and Luding [57] in dry granular jamming showing equivalence in jamming behavior between polydisperse and equivalent bidisperse systems. In this work, although we have focused on

the model systems of two species, the results can be used to qualitatively predict the rheology of polydisperse suspensions, which has many applications: industrial processing of slurries and muds, manufacturing of amorphous solid dispersions, and predicting the runout of geophysical flows comprising grains spanning many orders of magnitude [58].

Codes and scripts necessary to reproduce the results reported in this article are available on request.

#### ACKNOWLEDGMENTS

We acknowledge support from the Center for Hierarchical Materials Design (CHiMaD) under Award No. 70NANB19H005 (U.S. Department of Commerce) and from the Army Research Office under Grants No. W911NF-19-1-0245 and No. W911NF-21-2-0146. A.S. acknowledges Case Western Reserve University for start-up funding. C.N. thanks Eric Breard for pointing to Ref. [40] and acknowledges support from the Royal Academy of Engineering under the Research Fellowship scheme and from the Leverhulme Trust under Research Project under Grant No. RPG-2022-095. Part of this work made use of the High Performance Computing Resource in the Core Facility for Advanced Research Computing at Case Western Reserve University.

A.S. and C.N. contributed equally to this work.

#### APPENDIX: NUMBER OF PARTICLES IN EACH SIMULATION

Shown in Table I are the total number of particles and the number of large particles for each simulation reported in this article.

TABLE I. Details of system size and number of large particles in the simulation performed in this work.

Size ratio (total number of particles)	Volumetric mixing ratio	Number of large particles
2 (6000)	0.05	3177
2 (6000)	0.1	2489
2 (6000)	0.5	668
2 (6000)	0.8	183
2 (6000)	0.9	83
4 (6000)	0.05	917
4 (6000)	0.1	741
4 (6000)	0.5	93
4 (6000)	0.8	24
4 (6000)	0.9	11
6 (6000)	0.05	486
6 (6000)	0.1	241
6 (6000)	0.5	29
6 (6000)	0.8	8
6 (6000)	0.9	2
12 (12000)	0.05	132
12 (12000)	0.1	63
12 (12000)	0.5	29
12 (12000)	0.8	3
12 (12000)	0.9	3

- [1] C. Ness, R. Seto, and R. Mari, *Annu. Rev. Condens. Matter Phys.* **13**, 97 (2022).
- [2] J. F. Morris, *Annu. Rev. Fluid Mech.* **52**, 121 (2020).
- [3] A. Singh, *MRS Commun.* **13**, 971 (2023).
- [4] N. Roussel, A. Lemaître, R. J. Flatt, and P. Coussot, *Cem. Concr. Res.* **40**, 77 (2010).
- [5] E. Brown and H. M. Jaeger, *Rep. Prog. Phys.* **77**, 046602 (2014).
- [6] I. R. Peters, S. Majumdar, and H. M. Jaeger, *Nature (London)* **532**, 214 (2016).
- [7] A. Singh, S. Pednekar, J. Chun, M. M. Denn, and J. F. Morris, *Phys. Rev. Lett.* **122**, 098004 (2019).
- [8] B. M. Guy, J. A. Richards, D. J. M. Hodgson, E. Blanco, and W. C. K. Poon, *Phys. Rev. Lett.* **121**, 128001 (2018).
- [9] A. Singh, C. Ness, R. Seto, J. J. de Pablo, and H. M. Jaeger, *Phys. Rev. Lett.* **124**, 248005 (2020).
- [10] A. Singh, G. L. Jackson, M. van der Naald, J. J. de Pablo, and H. M. Jaeger, *Phys. Rev. Fluids* **7**, 054302 (2022).
- [11] R. Seto, R. Mari, J. F. Morris, and M. M. Denn, *Phys. Rev. Lett.* **111**, 218301 (2013).
- [12] M. Wyart and M. E. Cates, *Phys. Rev. Lett.* **112**, 098302 (2014).
- [13] A. Singh, R. Mari, M. M. Denn, and J. F. Morris, *J. Rheol.* **62**, 457 (2018).
- [14] B. M. Guy, M. Hermes, and W. C. K. Poon, *Phys. Rev. Lett.* **115**, 088304 (2015).
- [15] C. Ness and J. Sun, *Soft Matter* **12**, 914 (2016).
- [16] B. M. Guy, C. Ness, M. Hermes, L. J. Sawiak, J. Sun, and W. C. Poon, *Soft Matter* **16**, 229 (2020).
- [17] S. Pradeep, M. Nabizadeh, A. R. Jacob, S. Jamali, and L. C. Hsiao, *Phys. Rev. Lett.* **127**, 158002 (2021).
- [18] H. Van Damme, *Cem. Concr. Res.* **112**, 5 (2018).
- [19] R. Flatt, *Mater. Struct.* **37**, 289 (2004).
- [20] C. D. Cwalina and N. J. Wagner, *J. Rheol.* **60**, 47 (2016).
- [21] Y. Madraki, S. Hormozi, G. Ovarlez, E. Guazzelli, and O. Pouliquen, *Phys. Rev. Fluids* **2**, 033301 (2017).
- [22] Y. Madraki, G. Ovarlez, and S. Hormozi, *Phys. Rev. Lett.* **121**, 108001 (2018).
- [23] N. Malbranche, B. Chakraborty, and J. F. Morris, *J. Rheol.* **67**, 91 (2023).
- [24] S. Pednekar, J. Chun, and J. F. Morris, *J. Rheol.* **62**, 513 (2018).
- [25] A. Monti and M. E. Rosti, *Meccanica* **58**, 727 (2023).
- [26] N. Malbranche, A. Santra, B. Chakraborty, and J. F. Morris, *Front. Phys.* **10**, 946221 (2022).
- [27] M. Ramaswamy, I. Griniasty, D. B. Liarte, A. Shetty, E. Katifori, E. Del Gado, J. P. Sethna, B. Chakraborty, and I. Cohen, *J. Rheol.* **67**, 1189 (2023).
- [28] B. J. Maranzano and N. J. Wagner, *J. Chem. Phys.* **114**, 10514 (2001).
- [29] R. Farris, *Trans. Soc. Rheol.* **12**, 281 (1968).
- [30] P. M. Mwasame, N. J. Wagner, and A. N. Beris, *J. Rheol.* **60**, 225 (2016).
- [31] A. P. Shapiro and R. F. Probst, *Phys. Rev. Lett.* **68**, 1422 (1992).
- [32] J. Chong, E. Christiansen, and A. Baer, *J. Appl. Polym. Sci.* **15**, 2007 (1971).
- [33] H. A. Barnes, *J. Rheol.* **33**, 329 (1989).
- [34] P. Gondret and L. Petit, *J. Rheol.* **41**, 1261 (1997).
- [35] A. Poslinski, M. Ryan, R. Gupta, S. Seshadri, and F. Frechette, *J. Rheol.* **32**, 703 (1988).
- [36] B. J. Maranzano and N. J. Wagner, *J. Rheol.* **45**, 1205 (2001).
- [37] C. Chang and R. L. Powell, *J. Rheol.* **38**, 85 (1994).
- [38] C. Chang and R. L. Powell, *Phys. Fluids* **6**, 1628 (1994).
- [39] C. Chang and R. L. Powell, *J. Fluid Mech.* **253**, 1 (1993).
- [40] A.-B. Yu and N. Standish, *Ind. Eng. Chem. Res.* **30**, 1372 (1991).
- [41] F. Qi and R. I. Tanner, *Korea-Aust. Rheol. J.* **23**, 105 (2011).
- [42] C. Anzivino, M. Casiulis, T. Zhang, A. S. Moussa, S. Martiniani, and A. Zaccone, *J. Chem. Phys.* **158**, 044901 (2023).
- [43] C. Servais, R. Jones, and I. Roberts, *J. Food Eng.* **51**, 201 (2002).
- [44] M. Pishvaei, C. Graillat, P. Cassagnau, and T. McKenna, *Chem. Eng. Sci.* **61**, 5768 (2006).
- [45] I. Srivastava, S. A. Roberts, J. T. Clemmer, L. E. Silbert, J. B. Lechman, and G. S. Grest, *Phys. Rev. Res.* **3**, L032042 (2021).
- [46] J. C. Petit, N. Kumar, S. Luding, and M. Sperl, *Phys. Rev. Lett.* **125**, 215501 (2020).
- [47] R. Mari, R. Seto, J. F. Morris, and M. M. Denn, *Phys. Rev. E* **91**, 052302 (2015).
- [48] J. F. Brady and G. Bossis, *J. Fluid Mech.* **155**, 105 (1985).
- [49] R. C. Ball and J. R. Melrose, *Physica A (Amsterdam, Neth.)* **247**, 444 (1997).
- [50] P. A. Cundall and O. D. L. Strack, *Géotechnique* **29**, 47 (1979).
- [51] S. Luding, *Granular Matter* **10**, 235 (2008).
- [52] R. Mari, R. Seto, J. F. Morris, and M. M. Denn, *J. Rheol.* **58**, 1693 (2014).
- [53] I. M. Krieger and T. J. Dougherty, *Trans. Soc. Rheol.* **3**, 137 (1959).
- [54] A. J. Liu and S. R. Nagel, *Annu. Rev. Condens. Matter Phys.* **1**, 347 (2010).
- [55] X. Li, J. R. Royer, and C. Ness, *J. Fluid Mech.* **984**, A67 (2024).
- [56] K. W. Desmond and E. R. Weeks, *Phys. Rev. E* **90**, 022204 (2014).
- [57] V. Ogarko and S. Luding, *J. Chem. Phys.* **136**, 124508 (2012).
- [58] E. C. Breard, J. Dufek, S. Charbonnier, V. Gueugneau, T. Giachetti, and B. Walsh, *Nat. Commun.* **14**, 2079 (2023).